Dentomaxillofacial Radiology (2017) 46, 20160434

birpublications.org/dmfr

RESEARCH ARTICLE

The value of combining conventional, diffusion-weighted and dynamic contrast-enhanced MR imaging for the diagnosis of parotid gland tumours

Xiaofeng Tao, Gongxin Yang, Pingzhong Wang, Yingwei Wu, Wenjing Zhu, Huimin Shi, Xin Gong, Weiqing Gao and Qiang Yu

Department of Radiology, Ninth People's Hospital, School of Medicine, Shanghai Jiao Tong University, Shanghai, China

Objectives: The aim of this study was to determine the value of combining conventional MRI, diffusion-weighted imaging (DWI) and dynamic contrast-enhanced (DCE)-MRI in diagnosing solid neoplasms in the parotid gland.
Methods: A total of 148 subjects (101 subjects with benign and 47 subjects with malignant tumours) were evaluated with conventional MRI, DWI and DCE-MRI prior to surgery and pathologic verification. The items observed with conventional MRI included the shape, capsule and signal intensity of parotid masses. The apparent diffusion coefficient (ADC) was calculated from DWI that was obtained with a *b*-factor of 0 and 1000 $s\,mm^{-2}$. A time–intensity curve (TIC) was obtained from DCE-MRI.
Results: There were significant differences ($p < 0.01$) in the shape, capsule, ADC and TIC between benign and malignant parotid tumours. Irregular neoplasms without a capsule, ADC $<1.12 \times 10^{-3}\,mm^2\,s^{-1}$ and a plateau enhancement pattern were valuable parameters for predicting malignant neoplasms. A combination of all of these parameters yielded sensitivity, specificity, accuracy, positive-predictive value and negative-predictive value of 85.1%, 94.1%, 91.2%, 87.0% and 93.1%, respectively.
Conclusions: A combined analysis using conventional MRI, DWI and DCE-MRI is helpful in distinguishing benign from malignant tumours in the parotid gland.
Dentomaxillofacial Radiology (2017) **46**, 20160434. doi: 10.1259/dmfr.20160434

Cite this article as: Tao X, Yang G, Wang P, Wu Y, Zhu W, Shi H, et al. The value of combining conventional, diffusion-weighted and dynamic contrast-enhanced MR imaging for the diagnosis of parotid gland tumours. *Dentomaxillofac Radiol* 2017; **46**: 20160434.

Keywords: parotid gland; neoplasm; magnetic resonance imaging (MRI); diffusion-weighted MR imaging (DW-MRI); dynamic contrast enhanced MR imaging (DCE-MRI)

Introduction

Pre-operative prediction of malignant tumours in the parotid gland is clinically important because different surgical techniques are used for benign and malignant lesions.[1,2] Fine-needle aspiration cytology (FNAC), a minimally invasive method, is a useful tool in the pre-operative diagnosis of salivary gland lesions.[3,4] However, conclusive results cannot always be obtained with FNAC because of insufficient specimens. In some research, FNAC recognized malignancy in 72–84% of tumours.[5,6]

Some MRI features of parotid gland tumours obtained from conventional MRI, such as ill-defined margin and low signal intensity (SI) on T_2 weighted images (T2WIs), are highly suggestive of malignancy.[7] However, some investigators hold the opposite view, and the sensitivities and specificities of these findings have been reported as low and significantly overlapping.[8,9]

Correspondence to: Dr Qiang Yu. E-mail: yuqiang6155@163.com

Xiaofeng Tao and Qiang Yu are the funded for this work.
Xiaofeng Tao and Gongxin Yang are the joint first authors.
Received 11 November 2016; revised 8 March 2017; accepted 13 March 2017

Diffusion-weighted imaging (DWI) has been proven to be a potentially useful technique for evaluating the characteristics of head and neck neoplasms.[10–17] However, Habermann et al[18] concluded that there was an overlap of mean apparent diffusion coefficients (ADCs) within a group of benign and malignant tumours in the parotid gland. Thus, there was no consensus on the role of DWI in differentiating between benign and malignant parotid tumours.

The usefulness of dynamic contrast-enhanced (DCE)-MRI parameters and the high diagnostic value of the time–intensity curve (TIC) derived from DCE-MRI have been well documented in previous studies.[19–23] Recently, DCE-MRI has been used in combination with DWI for analyzing parotid gland tumours and has been shown to have a higher diagnostic value.[24,25] However, there are only a few reports for assessing the value of combining conventional MRI with DWI and DCE-MRI for determining the characteristics of parotid gland tumours.

The purpose of this study was to compare the different methods and determine the value of combining conventional MRI, DWI, and DCE-MRI for the diagnosis of parotid gland tumours.

Methods and materials

Patients

This retrospective study was approved by our hospital review committee. A total of 161 patients with parotid gland tumours were examined using conventional MRI, DWI and DCE-MRI from October 2004 to December 2012. Based on the results, 13 patients were excluded because of poor image quality (motion and susceptibility artefacts) or tumours that were too small to be measured on ADC maps. The remaining 148 patients comprised 87 males and 61 females who ranged in age from 13 to 86 years, with a mean age of 52 years. The final diagnoses were based on the pathological findings of the specimens obtained during surgical resection.

MRI examination

MRI examinations were performed using a 1.5-T MR scanner (Signa MR™; GE Medical System, Milwaukee, WI) with head and neck array coils. All of the axial conventional MRI, DWI and DCE-MRI examinations consisted of a 5-mm section thickness and a 1-mm intersection gap, 320 × 192 acquisition matrix and a 24 × 24-cm field of view. Axial T_1 weighted spin-echo sequences were performed with a repetition time (TR) of 540 ms and an echo time (TE) of 8.7 ms. Axial T_2 weighted fast spin-echo (FSE) sequences were performed with a TR of 4200 ms and a TE of 94.2 ms. Moreover, coronal T_2 weighted FSE sequences with 4-mm section thickness and a 1-mm intersection gap, 320 × 192 acquisition matrix and a 24 × 24-cm field of view were performed with a TR of 3420 ms and a TE of 80.4 ms. The fat suppression technique on T2WIs was used with the same parameters except a TR of 4440 ms.

DWI was performed using a spin-echo single-shot echoplanar imaging sequence in the axial plane with a TR of 3000 ms and a TE of 70 ms. Sensitizing diffusion gradients were applied sequentially in three directions with *b*-values between 0 and 1000 s mm^{-2}. ADC maps were automatically generated from DWI (FuncTool ADC package; GE Healthcare, Milwaukee WI).

Gadolinium diethylenetriamine pentaacetic acid (Magnevist®; Schering, Berlin, Germany) was administered intravenously at a rate of 2 mL s^{-1} (total dose, 0.1 mmol per kg of body weight) using a power injector, followed by a 20-mL saline flush. DCE-MRI was sequentially obtained prior to and after administration of the contrast material, and 40 consecutive data sets were acquired in 180–200 s within 8 sections. Parotid gland tumours were identified on axial T_1 weighted MRI, and the dynamic MRI was performed using FSE T_1 weighted images with a TR of 400–600 ms and a TE of 8–9.9 ms.

The total acquisition time for conventional MRI, DWI and DCE-MRI was approximately 25–30 min.

MRI evaluation

Conventional MRIs were interpreted, and consensus was achieved by two radiologists with more than 10 years' experience in head and neck MRI diagnosis who were blinded to the histopathologic results. The interpretation of the conventional MRI was based on the shape, capsule and SI of the tumours (Figures 1–3). The linear low signal around the tumour was regarded as a capsule on axial and coronal T2WIs. A partially encapsulated tumour on MRIs was also regarded as "with capsule". Because all of the tumours had a high SI compared with the adjacent muscles in the same section on T2WI, the signal of parotid gland masses was judged homogeneous or heterogeneous based on T2WI.

On axial DWI of the maximum diameter of the parotid tumours, a radiologist blinded to the histopathologic results manually drew a region of interest (ROI) within the solid part of the lesions (Figures 1–3), and the area of ROIs of each tumour was >35 mm^2. Based on the ROI, mean (±standard deviation) ADC was calculated from the following formula:

$$\mathrm{ADC} = \ln(S/S_0) \times (-1/b),$$

where S represents the SI after application of the diffusion gradient; S_0 represents SI with a *b*-value of 0 s mm^{-2} and b is the *b*-value.

To obtain the constructed TIC, the ROI was manually drawn for measurements of the SI by the same radiologist on an axial section of the maximum diameter of the parotid tumour. For cases in which the contrast enhancement was heterogeneous, the SIs of multiple areas were measured. We drew an ROI (approximately 20–40 mm^2) and kept dragging it over the enhanced part of the lesion until the TIC showed the most prominent enhancement. Then, the obtained TIC was selected as

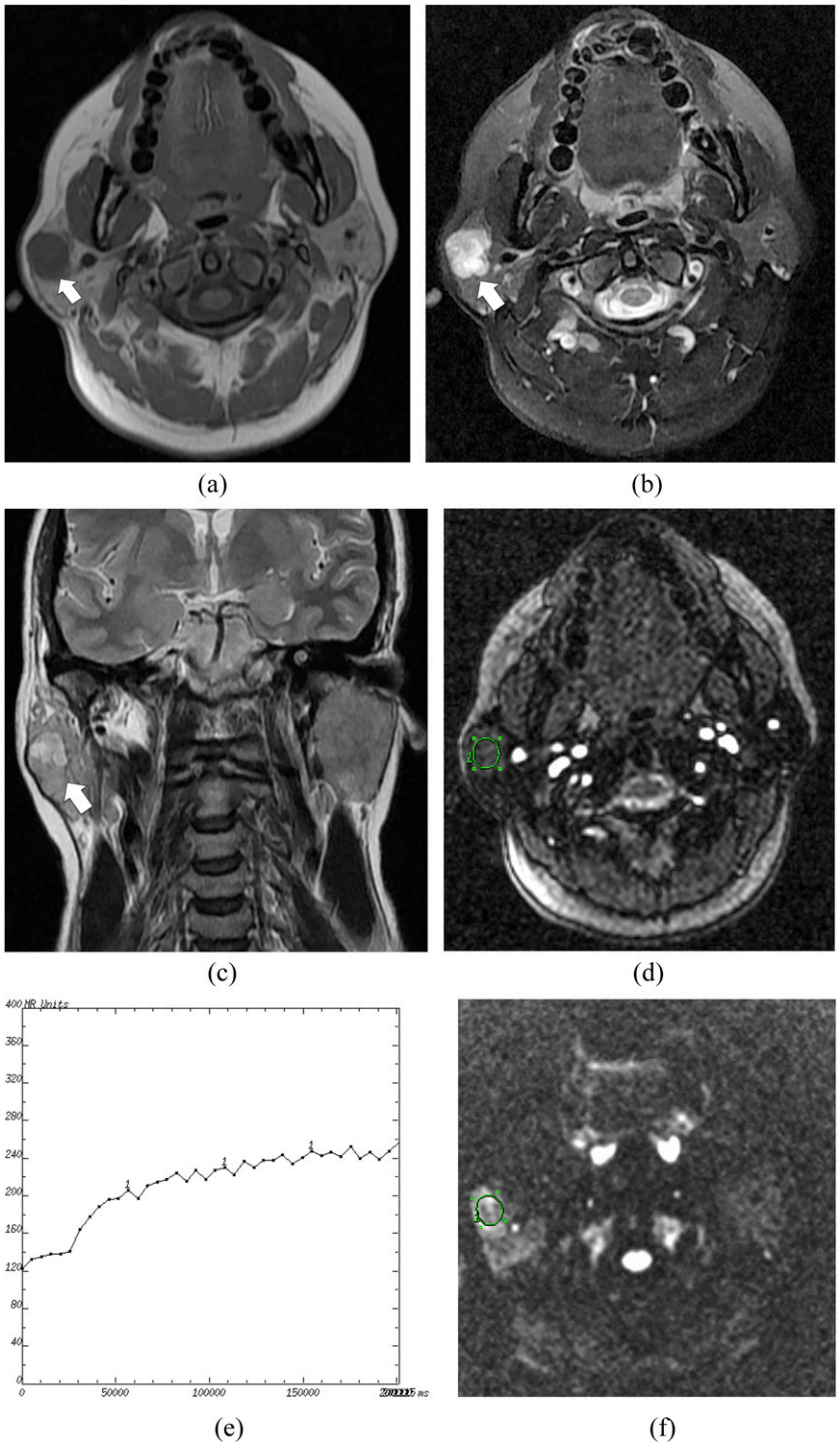

Figure 1 A pleomorphic adenoma of the right parotid gland in a 44-year-old female: (a) the axial T_1 weighted MR image shows a hypointense mass (arrow) in the right parotid gland. (b) The axial T_2 weighted MR image shows a heterogeneously hyperintense mass with an irregular shape (arrow). (c) The coronal T_2 weighted MR image shows a hypointense capsule around the mass (arrow). (d) The round cursor marks the region of interest (ROI) selected for signal intensity (SI) measurement with dynamic MRI. (e) The time–intensity curve shows a persistent enhancement pattern (Type A). (f) The diffusion-weighted image shows a relatively high SI mass. The round cursor marks the ROI selected for measurement of the apparent diffusion coefficient (ADC) value. The mean ADC value of this parotid tumour is 1.75×10^{-3} mm^2 s^{-1}.

the representation for each lesion. The vessels and cystic regions within the parotid tumours were avoided as much as possible.

The SI_{peak} was defined as the first signal intensity measurement that satisfied the inequality $SI > [0.9 (SI_{max} - SI_{pre})] + SI_{pre}$. The time to peak (TTP) represented

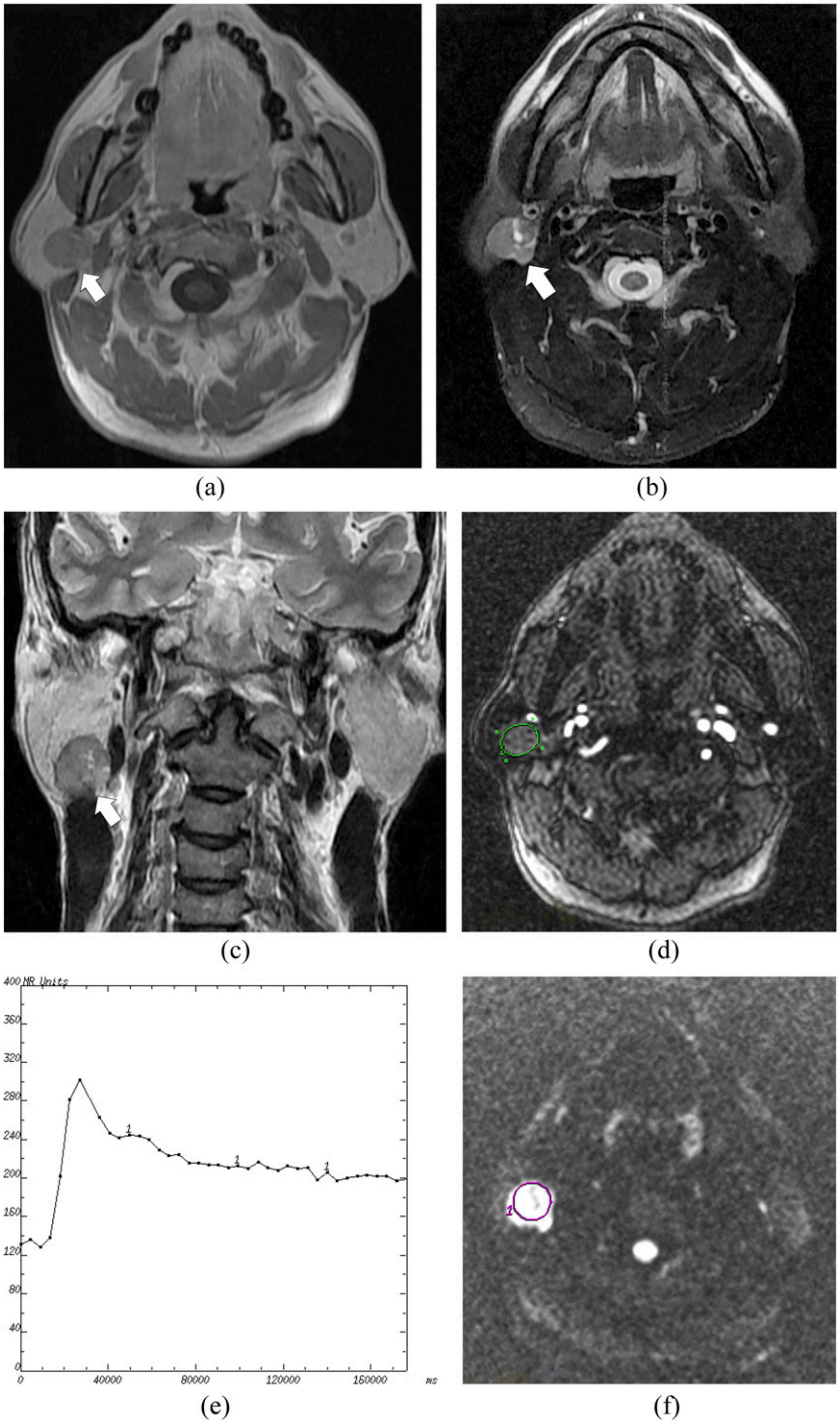

Figure 2 A Warthin's tumour of the right parotid gland in a 48-year-old male: (a) the axial T_1 weighted MR image shows an isointense signal mass with a round shape (arrow) in the right parotid gland. (b) The axial T_2 weighted MR image shows a relatively hyperintense mass (arrow). (c) The coronal T_2 weighted MR image shows a hypointense capsule around the mass (arrow). (d) The round cursor marks the region of interest (ROI) selected for the signal intensity (SI) measurement with dynamic MRI. (e) The time–intensity curve shows a washout enhancement pattern (Type B). (f) The diffusion-weighted image shows a high SI mass. The round cursor marks the ROI selected for measurement of the apparent diffusion coefficient (ADC) value. The mean ADC value of this tumour is measured as $0.74 \times 10^{-3}\,mm^2\,s^{-1}$.

the time that corresponded to the SI_{peak}. The SI_{pre} represented the pre-contrast signal intensity, the SI_{last} was the signal intensity at 180 s and the SI_{max} was defined as the signal intensity at maximal contrast enhancement. According to TTP and washout ratio (WR), the type of TIC was classified: $WR = (SI_{max} - SI_{last})/(SI_{max} - SI_{pre}) \times 100\%$. The thresholds of TTP and WR in differentiating benign

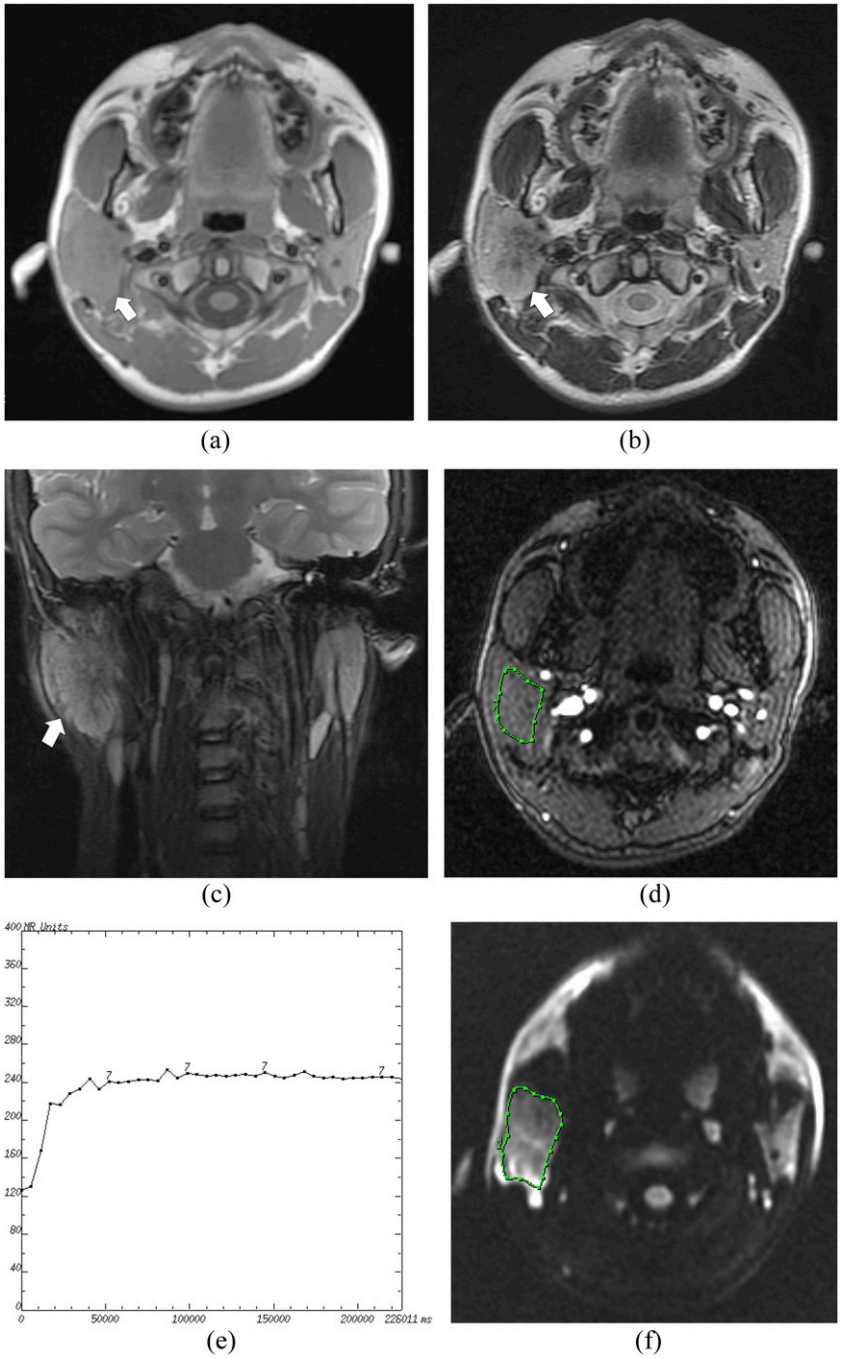

Figure 3 A mucoepidermoid carcinoma of the right parotid gland in a 15-year-old male: (a) the axial T_1 weighted MR image shows an isointense signal mass (arrow) in the right parotid gland with an irregular shape. (b) The axial T_2 weighted MR image shows a heterogeneously hyperintense mass (arrow). (c) The coronal T_2 weighted MR image shows no capsule around the mass (arrow). (d) The cursor marks the region of interest (ROI) selected for signal intensity (SI) measurement with dynamic MRI. (e) The time–intensity curve shows a plateau enhancement pattern (Type C). (f) The diffusion-weighted image shows a relatively high SI mass. The cursor marks the ROI selected for measurement of the apparent diffusion coefficient (ADC) value. The mean ADC value of this tumour is calculated as 1.01×10^{-3} mm^2 s^{-1}.

and malignant tumours would be obtained from our sample.

Statistical analysis

Statistical analyses were performed using the SPSS® v. 19.0 statistical software package (IBM Corp., New York, NY; formerly SPSS Inc., Chicago, IL). Logistic regression was used to analyze whether there were differences in shape, capsule and SI between benign and malignant tumours on the static MRI. Numeric data were reported as the mean ± standard deviation and 95% confidence interval. A non-parametric test (Mann–Whitney

Table 1 Histological results with apparent diffusion coefficient (ADC) values and time–intensity curve (TIC) patterns of parotid gland tumours

Pathology	*Number of cases*	b = *1000 (s/mm²)* *Mean ADC ± SD (10^{-3} mm²/s)*	*TIC pattern* *A*	*B*	*C*
Benign					
Pleomorphic adenoma	50	1.43 ± 0.26	41	1	8
Warthin's tumour	41	0.86 ± 0.13	1	35	5
Other benign epithelial tumours[a]	10	1.09 ± 0.22	2	5	3
Malignant					
Malignant epithelial tumours[b]	36	0.96 ± 0.20	6	2	28
Sarcoma[c]	4	0.76 ± 0.10		1	3
Lymphoma	7	0.77 ± 0.12		1	6

SD, standard deviation.
[a]Including myoepithelioma ($n = 2$), oncocytoma ($n = 2$) and basal cell adenoma ($n = 6$).
[b]Including adenoid cystic carcinoma ($n = 1$), malignant pleomorphic adenoma ($n = 6$), acinic cell carcinoma ($n = 4$), mucoepidermoid carcinoma ($n = 7$), metastatic carcinoma ($n = 2$), papillary cystadenocarcinoma ($n = 1$), tricholemmal carcinoma ($n = 1$), adenocarcinoma ($n = 3$), squamous cell carcinoma ($n = 6$) and lymphoepithelial carcinoma ($n = 5$).
[c]Including malignant fibrous histiocytoma ($n = 1$), leiomyosarcoma ($n = 1$), malignant haemangiopericytoma ($n = 1$) and unclassified sarcoma ($n = 1$).

U test) was used to compare the mean ADCs, and the χ^2 test was used to compare the TIC patterns between benign and malignant tumours. Using SPSS and receiver-operating characteristic curve analysis of mean ADC, TTP and WR, the diagnostic threshold for differentiating between benign and malignant conditions was obtained.

Different combinations of conventional MRI, mean ADCs and TIC of parotid tumours were evaluated with regression coefficients and constants that were obtained from binary logistic regression analysis with a cut-off point of 0.5. The specificity, sensitivity, accuracy, positive-predictive value (PPV) and negative-predictive value (NPV) were calculated based on the corresponding threshold value and the Youden index of different combinations. A p-value < 0.05 indicated a significant difference.

Results

A total of 148 patients diagnosed with parotid neoplasms were evaluated, including 101 patients with benign tumours (Figures 1 and 2) and 47 patients with malignant tumours (Figure 3). 27 patients have bilateral tumours or multiple tumours, including 22 Warthin's tumours (17 bilateral and 4 multiple on the left and 1 multiple on the right), 1 oncocytoma (bilateral) and 4 lymphomas (2 bilateral and 2 multiple on the right). Only the largest and well-displayed tumour was included in the study. The shortest diameter of each tumour included was >1 cm.

The histopathologic distributions of all the parotid gland tumours are shown in Table 1. The shapes and capsules of the benign and malignant tumours in the parotid gland were significantly different ($p < 0.01$, respectively) (Table 2). No significant difference was found in the SI of benign tumours and malignant lesions ($p = 0.133$).

The mean ADCs of malignant tumours [$(0.91 \pm 0.20) \times 10^{-3}$ mm² s^{-1}] was significantly lower ($p < 0.001$) than those of benign tumours [$(1.16 \pm 0.34) \times 10^{-3}$ mm² s^{-1}] (Figure 4A). Analysis of the receiver-operating characteristic curve (Figure 4B) yielded a cut-off point for the mean ADC of 1.12×10^{-3} mm² s^{-1} with 91.5% sensitivity, 51.5% specificity, 64.2% accuracy, 46.7% PPV and 92.9% NPV (Table 3).

The thresholds of TTP and WR in differentiating benign and malignant tumours were 58 ms and 22.6%, respectively. The TIC types of parotid tumours were classified based on TTP and WR: Type A (Figure 1E), the persistent pattern (TTP ≥ 58 ms); Type B (Figure 2E), the washout pattern (TTP < 58 ms and WR ≥ 22.6%); and Type C (Figure 3E), the plateau pattern (TTP < 58 ms and WR < 22.6%). The distribution of TIC patterns of the 148 parotid tumours is shown in Table 1. If we regarded the tumours with TIC Types A and B as benign and Type C as malignancy, the sensitivity, specificity, accuracy, PPV and NPV would be 78.7%, 84.2%, 82.4%, 69.8% and 89.5%, respectively (Table 3).

Table 2 Static MR findings of parotid gland tumours

MR findings	*Malignant (n = 47)*	*Benign (n = 101)*	p-*value*	*OR*	*95% CI*
Shape					
Round or oval	2	60	0.001[a]	12.983	2.679–62.928
Irregular	45	41			
Capsule					
Yes	9	88	0.000[a]	13.879	5.09–37.842
No	38	13			
Signal					
Homogeneous	7	37	0.133	2.498	0.757–8.235
Heterogeneous	40	64			

CI, confidence interval; OR, odds ratio.
[a]*p*-value shows statistical significance ($p < 0.05$).

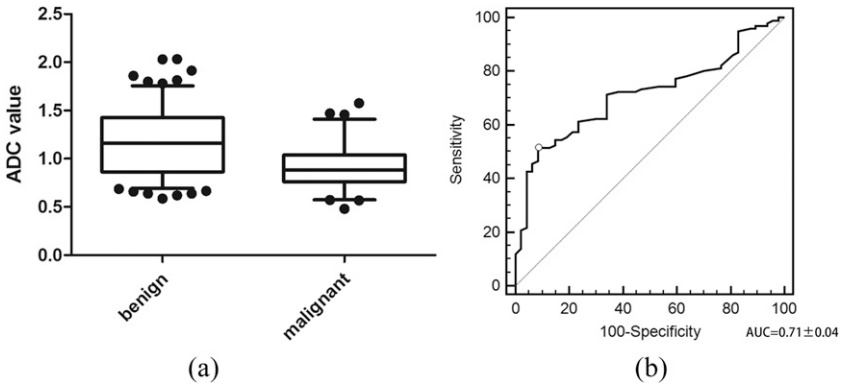

Figure 4 Discrimination of mean apparent diffusion coefficient (ADC) values between benign and malignant tumours: (a) the mean ADC value of malignant tumours [$(0.91 \pm 0.20) \times 10^{-3}\,mm^2\,s^{-1}$] is significantly lower than that of benign masses [$(1.16 \pm 0.34) \times 10^{-3}\,mm^2\,s^{-1}$] ($p < 0.001$). (b) The receiver-operating characteristic of mean ADC values for use in differentiating between malignancies and benign tumours. The area under the curve (AUC) is 0.71 ± 0.04, and a cut-off point of $1.12 \times 10^{-3}\,mm^2\,s^{-1}$ for the ADC value is obtained.

According to the above-mentioned outcomes, four items, irregular form without capsule, mean ADC $<1.12 \times 10^{-3}\,mm^2\,s^{-1}$ and TIC Type C were valuable for predicting malignancy. Table 4 shows the results of the logistic regression in different combinations. On the basis of the constants and regression coefficients of the four items (Table 4), the Logistic P for each parotid tumour, which represents the risk of it being malignant, can be calculated with the following formula:

Logistic P for each parotid tumour = constant + b_1 × shape + b_2 × capsule + b_3 × mean ADC value + b_4 × TIC

Shape : irregular form = 1; round or oval form = 0

Capsule : no capsule = 1; capsule = 0

Mean ADC value : mean ADC value less than 1.12 $\times 10^{-3}$ mm^2/s = 1; mean ADC value more than 1.12 $\times 10^{-3}$ mm^2/s = 0

TIC : TIC C = 1; TIC A or B = 0

b_1, b_2, b_3, b_4 = regression coefficients of each item.

Table 3 shows the diagnostic ability of the four items alone and in various combinations with the Youden index, sensitivity, specificity, accuracy, PPV and NPV.

Discussion

Conventional MRI has been extensively used for the assessment of various parotid gland conditions by revealing their morphological features. MRI findings referring to T_2 hypointensity, ill-defined margins, diffuse growth, infiltration of the subcutaneous tissue and lymphadenopathy have been used to predict parotid malignancies.[7] However, some investigators[8,9] have noted that the tumour margins and SI have not produced differential diagnoses of parotid gland tumours and have lower sensitivities and specificities. The present study indicated that the shape and capsule of parotid tumours were significantly different between benign and malignant tumours. In addition, our results supported the viewpoint that there was no significant difference in the SIs of benign and malignant parotid neoplasms.

Table 3 The diagnostic value of various combinations in distinguishing between benign and malignant neoplasms

Items	*Youden index*	*Sensitivity*	*Specificity*	*Accuracy*	*PPV*	*NPV*
Shape	0.551	95.7% (45/47)	59.4% (60/101)	70.9% (105/148)	52.3% (45/86)	96.8% (60/62)
Capsule	0.68	80.9% (38/47)	87.1% (88/101)	85.1% (126/148)	74.5% (38/51)	90.7% (88/97)
Mean ADC value	0.43	91.5% (43/47)	51.5% (52/101)	64.2% (95/148)	46.7% (43/92)	92.9% (52/56)
TIC	0.629	78.7% (37/47)	84.2% (85/101)	82.4% (122/148)	69.8% (37/53)	89.5% (85/95)
Shape + capsule	0.624	72.3% (34/47)	90.1% (91/101)	86.5% (128/148)	78.7% (37/47)	90.1% (91/101)
Shape + ADC	0.773	87.2% (41/47)	90.1% (91/101)	89.2% (132/148)	80.4% (41/51)	93.8% (91/97)
Shape + TIC	0.728	78.7% (37/47)	94.1% (95/101)	89.2% (132/148)	86.0% (37/43)	90.5% (95/152)
Capsule + ADC	0.686	74.5% (35/47)	94.1% (95/101)	87.8% (130/148)	85.4% (35/41)	94.1% (95/101)
Capsule + TIC	0.682	70.2% (33/47)	98.0% (99/101)	89.2% (132/148)	97.1% (34/35)	87.6% (99/113)
ADC + TIC	0.695	74.5% (35/47)	95.0% (96/101)	88.5% (131/148)	87.5% (35/40)	88.9% (96/108)
Shape + capsule + ADC	0.773	87.2% (41/47)	90.1% (91/101)	89.2% (132/148)	80.4% (41/51)	93.8% (91/97)
Shape + capsule + TIC	0.728	78.7% (37/47)	94.1% (95/101)	89.2% (132/148)	86.0% (37/43)	90.5% (95/105)
Shape + ADC + TIC	0.773	87.2% (41/47)	90.1% (91/101)	89.2% (132/148)	80.4% (41/51)	93.8% (91/97)
Capsule + ADC + TIC	0.743	87.2% (41/47)	87.1% (88/101)	87.2% (129/148)	75.9% (41/54)	93.6% (88/94)
Combination of all items	0.792	85.1% (40/47)	94.1% (95/101)	91 2% (135/148)	87.0% (40/46)	93.1% (95/102)

ADC, apparent diffusion coefficient; NPV, negative-predictive value; PPV, positive-predictive value; TIC, time–intensity curve.

Table 4 The results of comprehensive analysis of MRI data with logistic regression

		Coefficient of each item			
Combinations	*Constant*	*Shape*	*Capsule*	*ADC value*	*TIC*
Shape + capsule	−3.94	2.568	2.639		
Shape + ADC	−6.46	4.403		3.472	
Shape + TIC	−4.58	3.316			2.823
Capsule + ADC	−4.095		3.362	2.449	
Capsule + TIC	−3.161		2.856		2.414
ADC + TIC	−4.223			2.709	3.176
Shape + capsule + ADC	−6.479	3.421	2.257	3.08	
Shape + capsule + TIC	−4.427	2.246	2.153		2.295
Shape + ADC + TIC	−7.139	3.904		3.289	2.675
Capsule + ADC + TIC	−4.91		2.757	2.461	2.511
Combination of all items	−6.883	3.059	1.727	3.061	2.297

ADC, apparent diffusion coefficient; TIC, time–intensity curve.

Among the conventional MRI signs of parotid gland neoplasms, the neoplastic capsule seems to be more significant than the neoplastic shape in differentiating between benign and malignant parotid tumours.

Theoretically, DWI can reflect tumour cellularity, mitosis and nuclear contour-based differences in the molecular translational motion of water. The role of DWI in differentiating between benign and malignant head and neck lesions has been reported in the literature.[10–18,26–28] Most of these studies demonstrated that the mean ADCs of malignant tumours were substantially lower than the mean ADCs of benign lesions,[10,11,13,14,16,17,26,28] although some investigators found no difference between benign and malignant tumours.[12,27] Our results were in concordance with most previous investigations. However, the specificity and accuracy of DWI are relatively lower because Warthin's tumours usually have lower mean ADCs. In addition, Habermann et al[18] reported that there was an overlap of mean ADCs not only between benign and malignant tumours but also within parotid benign or malignant tumours. A possible explanation for those overlaps is that the ADCs of tissues vary depending on the microstructures, physiologic states[14] and cellularity[11,28] of the tissues. The results of the present study indicate that the specificity and accuracy of mean ADCs were relatively lower among all of the observed items. Therefore, it is inappropriate to focus only on the mean ADCs of parotid neoplasms for MRI diagnosis.

DCE-MRI can reveal haemodynamic information, and the effectiveness for distinguishing between benign and malignant salivary gland tumours has been confirmed by some studies.[20–23] Hisatomi et al[21] and Yabuuchi et al[23] found that DCE-MRI parameters and TIC patterns were useful in the differential diagnosis of salivary gland tumours based on the combined assessment of TTP and WR. Both studies[21,23] indicated that a TTP of 120 s allowed for the differentiation of a malignant carcinoma from a benign pleomorphic adenoma but not from a Warthin's tumour, whereas a WR of 30% enabled the differentiation between a malignant tumour and a Warthin's tumour. In the present study, we utilized the TIC classifications based on 58 ms of TTP and 22.6% of WR, which were obtained from these data, and the shorter scanning time may have induced the differences from those reports. Although DCE-MRI was valuable for predicting whether a parotid gland lesion was benign or malignant, the misdiagnosis and overlap between benign (TIC Type A and Type B) and malignant (Type C) tumours could not be avoided in our study, especially for TIC Type C neoplasms. On the other hand, when we compared DCE-MRI with DWI, we found that the specificity and accuracy of the former is higher than that of the latter in distinguishing between benign tumours and malignancies.

Diagnostic values among the different items (neoplastic shape, capsule, mean ADCs and TIC) vary. By comparison, we noticed that the neoplastic capsule was most useful for the differential diagnosis of parotid gland tumours (0.68 Youden index), followed by the TIC (0.63 Youden index), neoplastic shape (0.55 Youden index) and mean ADC (0.43 Youden index).

A combination of DCE-MRI and DWI has been confirmed to improve the MRI performance in distinguishing between benign and malignant parotid gland tumours and characterizing the different histological types of benign tumours.[24,25] In the present study, we found that a combination of DCE-MRI and DWI is superior to either DCE-MRI or DWI alone in the identification of parotid benign tumours and malignancies. In addition to both DWI and DCE-MRI, we added conventional MRI items into the present study. The different combinations among conventional MRI (neoplastic shape and capsule), DWI and DCE-MRI had different roles and weights in the identification of parotid benign tumours and malignancies. To indicate these differences and weights, we utilized regression coefficients and constants to process and analyze our data. To our knowledge, there have been few prior investigations of this method. Our results indicated that any combination of conventional MRI and functional MRI (mean ADCs and TIC), such as shape + ADCs; shape + TIC; shape + capsule + ADCs; ADCs + TIC + shape or capsule; and shape + capsule + ADCs + TIC, was better than either conventional MRI or DWI and DCE-MRI alone. We believe that a multiview

synthesis analysis combining conventional MRI, DWI and DCE-MRI may be considered a comprehensive reflection with regard to the gross morphology, cellularity and haemodynamics of parotid tumour tissues. In addition, the combination may provide comprehensive information reflecting the physiologic and pathological states of biologic tissues and improve the accuracy of diagnosis. A recent research from Yuan et al[29] demonstrated that the diagnostic value of MRI would increase when DWI is applied in combination with morphological analyses exclusive of DCE-MRI, which did not coincide exactly with our result. We think the method of analysis may induce differences. In the Yuan et al[29] study, each parameter could not objectively show its weight for predicting malignant neoplasms in various combinations and showed relatively low sensitivity (32.35–54.05%). In addition, our data revealed that the diagnostic value of the combination of all the four items (neoplastic shape, capsule, ADC and TIC) in differentiating benign from malignant parotid tumours seemed to be approximately the highest of all the combinations (0.792 Youden index). From these outcomes, we can infer that the diagnostic roles of conventional MRI should not be ignored when we gradually and extensively use DWI and DCE-MRI for the assessment of salivary gland neoplasms. Rather, the combination of conventional and functional MRI should be emphasized because it may increase the diagnostic accuracy of parotid gland tumours.

The main limitations of the present study are as follows. (1) We did not consider the gland signal change with patient age. (2) The ADC value varies depending on the equipment and hospital imaging method. (3) The findings shown on conventional MRI and functional MRI (DCE and DWI) may overlap between parotid benign and malignant tumours, and these could result in an incorrect diagnosis. (4) In the present study, the DWI and DCE-MRI for 8% of the subjects (13 of 161 subjects) were of low quality and could not be evaluated. The main reasons for the poor quality images were motion and susceptibility artefacts.

Conclusions

In conclusion, if parotid gland tumours are shown on MRI as being of irregular shape, with no capsule, mean ADC $<1.12\times10^{-3}\,mm^2\,s^{-1}$ and TIC Type C, a malignancy should be strongly considered. An evaluation combining MRI morphologic findings (shape and capsule) and functional MRI (mean ADCs and TIC) in the diagnosis of parotid gland neoplasms is superior to that of either conventional MRI or functional MRI alone. The combination would compensate for the shortcomings of each and thus improve the diagnostic accuracy for differentiating benign and malignant parotid tumours.

References

1. Scianna JM, Petruzzelli GJ. Contemporary management of tumors of the salivary glands. *Curr Oncol Rep* 2007; **9**: 134–8. doi: https://doi.org/10.1007/s11912-007-0011-6
2. Swoboda H, Franz P. Salivary gland tumors. Clinical aspects and therapy. [In German.] *Radiologe* 1994; **34**: 232–8.
3. Mihashi H, Kawahara A, Kage M, Kojiro M, Nakashima T, Umeno H, et al. Comparison of preoperative fine-needle aspiration cytology diagnosis and histopathological diagnosis of salivary gland tumors. *Kurume Med J* 2006; **53**: 23–7. doi: https://doi.org/10.2739/kurumemedj.53.23
4. Das DK, Petkar MA, Al-Mane NM, Sheikh ZA, Mallik MK, Anim JT. Role of fine needle aspiration cytology in the diagnosis of swellings in the salivary gland regions: a study of 712 cases. *Med Princ Pract* 2004; **13**: 95–106.
5. Zbären P, Nuyens M, Loosli H, Stauffer E. Diagnostic accuracy of fine-needle aspiration cytology and frozen section in primary parotid carcinoma. *Cancer* 2004; **100**: 1876–83.
6. Al-Khafaji BM, Nestok BR, Katz RL. Fine-needle aspiration of 154 parotid masses with histologic correlation: ten-year experience at the University of Texas M. D. Anderson Cancer Center. *Cancer* 1998; **84**: 153–9.
7. Christe A, Waldherr C, Hallett R, Zbaeren P, Thoeny H. MR imaging of parotid tumors: typical lesion characteristics in MR imaging improve discrimination between benign and malignant disease. *AJNR Am J Neuroradiol* 2011; **32**: 1202–7. doi: https://doi.org/10.3174/ajnr.a2520
8. Yousem DM, Kraut MA, Chalian AA. Major salivary gland imaging. *Radiology* 2000; **216**: 19–29. doi: https://doi.org/10.1148/radiology.216.1.r00jl4519
9. Joe VQ, Westesson PL. Tumors of the parotid gland: MR imaging characteristics of various histologic types. *AJR Am J Roentgenol* 1994; **163**: 433–8. doi: https://doi.org/10.2214/ajr.163.2.8037045
10. Eida S, Sumi M, Sakihama N, Takahashi H, Nakamura T. Apparent diffusion coefficient mapping of salivary gland tumors: prediction of the benignancy and malignancy. *AJNR Am J Neuroradiol* 2007; **28**: 116–21.
11. Lyng H, Haraldseth O, Rofstad EK. Measurement of cell density and necrotic fraction in human melanoma xenografts by diffusion weighted magnetic resonance imaging. *Magn Reson Med* 2000; **43**: 828–36. doi: https://doi.org/10.1002/1522-2594(200006)43:6<828::aid-mrm8>3.3.co;2-g
12. Matsushima N, Maeda M, Takamura M, Takeda K. Apparent diffusion coefficients of benign and malignant salivary gland tumors. Comparison to histopathological findings. *J Neuroradiol* 2007; **34**: 183–9.
13. Motoori K, Yamamoto S, Ueda T, Nakano K, Muto T, Nagai Y, et al. Inter- and intratumoral variability in magnetic resonance imaging of pleomorphic adenoma: an attempt to interpret the variable magnetic resonance findings. *J Comput Assist Tomogr* 2004; **28**: 233–46. doi: https://doi.org/10.1097/00004728-200403000-00014
14. Wang J, Takashima S, Takayama F, Kawakami S, Saito A, Matsushita T, et al. Head and neck lesions: characterization with diffusion-weighted echo-planar MR imaging. *Radiology* 2001; **220**: 621–30. doi: https://doi.org/10.1148/radiol.2202010063
15. Wang P, Yang J, Yu Q, Ai S, Zhu W. Evaluation of solid lesions affecting masticator space with diffusion-weighted MR imaging. *Oral Surg Oral Med Oral Pathol Oral Radiol Endod* 2010; **109**: 900–7. doi: https://doi.org/10.1016/j.tripleo.2010.01.005
16. Yerli H, Aydin E, Haberal N, Harman A, Kaskati T, Alibek S. Diagnosing common parotid tumours with magnetic resonance imaging including diffusion-weighted imaging *vs* fine-needle aspiration cytology: a comparative study. *Dentomaxillofac Radiol* 2010; **39**: 349–55. doi: https://doi.org/10.1259/dmfr/15047967

17. Yoshino N, Yamada I, Ohbayashi N, Honda E, Ida M, Kurabayashi T, et al. Salivary glands and lesions: evaluation of apparent diffusion coefficients with split-echo diffusion-weighted MR imaging—initial results. *Radiology* 2001; **221**: 837–42.
18. Habermann CR, Arndt C, Graessner J, Diestel L, Petersen KU, Reitmeier F, et al. Diffusion-weighted echo-planar MR imaging of primary parotid gland tumors: is a prediction of different histologic subtypes possible? *AJNR Am J Neuroradiol* 2009; **30**: 591–6. doi: https://doi.org/10.3174/ajnr.a1412
19. Eida S, Sumi M, Nakamura T. Multiparametric magnetic resonance imaging for the differentiation between benign and malignant salivary gland tumors. *J Magn Reson Imaging* 2010; **31**: 673–9. doi: https://doi.org/10.1002/jmri.22091
20. El Shahat HM, Fahmy HS, Gouhar GK. Diagnostic value of gadolinium-enhanced dynamic MR imaging for parotid gland tumors. *Egyptian Journal of Radiology and Nuclear Medicine* 2013; **44**: 203–7. doi: https://doi.org/10.1016/j.ejrnm.2013.02.007
21. Hisatomi M, Asaumi J, Yanagi Y, Unetsubo T, Maki Y, Murakami J, et al. Diagnostic value of dynamic contrast-enhanced MRI in the salivary gland tumors. *Oral Oncol* 2007; **43**: 940–7. doi: https://doi.org/10.1016/j.oraloncology.2006.11.009
22. Matsuzaki H, Yanagi Y, Hara M, Katase N, Asaumi J, Hisatomi M, et al. Minor salivary gland tumors in the oral cavity: diagnostic value of dynamic contrast-enhanced MRI. *Eur J Radiol* 2012; **81**: 2684–91. doi: https://doi.org/10.1016/j.ejrad.2011.11.005
23. Yabuuchi H, Fukuya T, Tajima T, Hachitanda Y, Tomita K, Koga M. Salivary gland tumors: diagnostic value of gadolinium-enhanced dynamic MR imaging with histopathologic correlation. *Radiology* 2003; **226**: 345–54. doi: https://doi.org/10.1148/radiol.2262011486
24. Lechner Goyault J, Riehm S, Neuville A, Gentine A, Veillon F. Interest of diffusion-weighted and gadolinium-enhanced dynamic MR sequences for the diagnosis of parotid gland tumors. *J Neuroradiol* 2011; **38**: 77–89. doi: https://doi.org/10.1016/j.neurad.2009.10.005
25. Yabuuchi H, Matsuo Y, Kamitani T, Setoguchi T, Okafuji T, Soeda H, et al. Parotid gland tumors: can addition of diffusion-weighted MR imaging to dynamic contrast-enhanced MR imaging improve diagnostic accuracy in characterization? *Radiology* 2008; **249**: 909–16. doi: https://doi.org/10.1148/radiol.2493072045
26. Inci E, Hocaoğlu E, Kiliçkesmez Ö, Aydin S, Cimilli T. Quantitative diffusion-weighted MR imaging in the differential diagnosis of parotid gland tumors: is it a useful technique?. *Turkiye Klinikleri J Med Sci* 2010; **30**: 1339–45.
27. Sakamoto J, Yoshino N, Okochi K, Imaizumi A, Tetsumura A, Kurohara K, et al. Tissue characterization of head and neck lesions using diffusion-weighted MR imaging with SPLICE. *Eur J Radiol* 2009; **69**: 260–8.
28. Uhl M, Altehoefer C, Kontny U, Il'yasov K, Buchert M, Langer M. MRI-diffusion imaging of neuroblastomas: first results and correlation to histology. *Eur Radiol* 2002; **12**: 2335–8. doi: https://doi.org/10.1007/s00330-002-1310-9
29. Yuan Y, Tang W, Tao X. Parotid gland lesions: separate and combined diagnostic value of conventional MRI, diffusion-weighted imaging and dynamic contrast-enhanced MRI. *Br J Radiol* 2016; **89**: 20150912. doi: https://doi.org/10.1259/bjr.20150912